A Competitive-Aging Method for Quantitative Genetic Analysis of the Chronological Lifespan of *Saccharomyces cerevisiae*

J. Abraham Avelar-Rivas[1], Michelle Munguía-Figueroa[1], Alejandro Juárez-Reyes[1], Erika Garay[1], Sergio E. Campos[1], Noam Shoresh[2] & Alexander DeLuna[1,*]

[1] *Centro de Investigación y de Estudios Avanzados del IPN, Unidad de Genómica Avanzada (Langebio), 36824 Irapuato, Guanajuato, Mexico.*
[2] *Broad Institute of MIT and Harvard, Cambridge, MA 02142, USA.*

*Corresponding author: alexander.deluna@cinvestav.mx

Author's emails:
J. Abraham Avelar-Rivas (jesus.avelar@cinvestav.mx)
Michelle Munguía-Figueroa (michelle.munguia@cinvestav.mx)
Alejandro Juárez-Reyes (alejandro.juarez@cinvestav.mx)
Erika Garay (egaray.gar@gmail.com)
Sergio E. Campos (sergio.e.campos@cinvestav.mx)
Noam Shoresh (noamshoresh@gmail.com)
Alexander DeLuna (alexander.deluna@cinvestav.mx)

Type of manuscript: Research Practice

Keywords: Post-mitotic aging; Genetic analysis; High-throughput screening; Gene-drug interactions

ABSTRACT

The chronological lifespan of budding yeast is a model of aging and age-related diseases. This paradigm has recently allowed genome-wide screening of genetic factors underlying post-mitotic viability in a simple unicellular system, which underscores its potential to describe the aging process in a systematic manner. However, results from different large-scale studies show little overlap and lack enough quantitative resolution to derive interactions of genetic aging factors with the environment. Here, we present a standardized, replicable, and parallelizable method to quantify the chronological-lifespan effects of gene deletions. We estimate the relative survival of stationary-phase cells by recurrently outgrowing co-cultures of wild-type and mutant strains expressing different fluorescent proteins. Importantly, we introduce a model to estimate the association between death rates and fluorescent signals, accounting for differences in growth rate and experimental batch effects. We describe the experimental procedure—from data acquisition to calculation of relative survivorship—for nine deletion strains and contrast replicability of our method with an established parallel approach. Furthermore, we apply our strategy to quantitatively characterize the gene-drug interactions of 76 deletion strains subjected to a lifespan-extending pharmacological treatment. Our competitive-aging approach with multiple-regression modeling provides a powerful screening platform to identify aging factors and their interactions with pharmacological interventions.

INTRODUCTION

A major challenge in aging research is to describe the way in which different genetic pathways and biochemical processes mediating aging are interconnected to one another and the environment [1,2]. Simple cellular models provide a starting point to grant a systems-level understanding of aging, in which the lifespan phenotype is addressed as a complex trait resulting from the action of multiple genes, cellular processes, environmental factors, and their interactions.

The chronological lifespan (CLS) of *Saccharomyces cerevisiae* is used to describe genetic, nutrimental, and pharmacological factors underlying survivorship of post-mitotic, non-dividing cells [3]. The budding yeast's replicative-lifespan and CLS are simple experimental models that have been used to reveal the conserved lifespan-extending effects of reduced TOR and RAS/PKA signaling, as well as the anti-aging effect of rapamycin, spermidine, and caloric restriction [3–6]. Traditionally, the CLS of a yeast-cell population is measured by counting colony-forming units from samples of a long-term stationary-phase culture [7,8]. More recently, large-scale screening approaches have been implemented to screen for genetic aging factors in yeast. These studies provide unbiased catalogues of CLS mutant phenotypes [9–13], mutants with diminished or enhanced response to dietary restriction or nutrient limitation [14,15], and CLS phenotypes of collections of wild isolates and lines derived from biparental crosses [16].

A current limitation of large-scale CLS phenotyping in yeast is that available screens have resulted in a large fraction of false positive hits when further confirmed by smaller-scale approaches, ranging from 50% to 94% [9–13]. In addition, comparisons of different

large-scale studies show that there is little overlap among the identified genetic factors. While this may be explained in part by differences in genotypic background, media composition, and subtle environmental variations [17], the large fraction of false positives and little overlap may also suggest that available large-scale CLS phenotyping approaches are still lacking enough technical replicability. Moreover, changes in specific controlled and uncontrolled environmental conditions are known to be important modifiers of CLS phenotypes and may be confounding causes of aging [12,17–20]. Hence, a combination of high throughput and good resolution is needed to correctly determine not only genetic aging factors, but also to quantitatively derive their interactions with nutrimental, chemical, or pharmacological environments. This poses an important technical challenge, given that the number of experiments scales exponentially while describing genetic and environmental interactions based on phenotypic measurements.

In this study, we describe a novel multiple regression modeling approach to analyze measurements from a previously introduced competition-based method for quantitative large-scale genetic analysis of CLS in yeast [13]. Systematic analyses of the method's replicability and scripts to quantify CLS of strains aging in competition with a wild-type reference are also provided. Importantly, this previous study assumed that mutant strains had no effects in doubling time, which biased relative-survivorship measurements of slow-growing strains. For nine knockout strains, we compare the replicability of our results with those obtained with a useful parallelizable approach based on outgrowth kinetics [21,22]. Finally, we take advantage of our improved method to derive gene-environment interactions by measuring the relative effects on survival of metformin in 76 single-gene deletion strains, revealing some of the genes that mediate

longevity by metformin in yeast. We discuss the potential of competitive-aging screening to describe not only interactions between thousands of genes and different environmental factors, but also large numbers of genetic interactions underlying aging and longevity in yeast.

MATERIALS AND METHODS

Strains and media. Nine single-gene deletion strains targeting *ATG1*, *HAP3*, *MSN2*, *MSN4*, *RAS2*, *RIM15*, *RPS16A*, *STE12*, and *SWR1* were generated *de novo* by PCR-based gene replacement in the YEG01-RFP background [13] using the *natMX4* module from pAG25 (Euroscarf). In addition, two isogenic reference strains were generated over the YEG01-RFP and YEG01-CFP backgrounds by deleting the neutral *HO* locus. Lithium-acetate transformation and 100 µg/ml clonNAT (Werner BioAgents) were used. The resulting strains were *MAT*-α *x*Δ*::natMX4 PDC1-RFP.CaURA3MX4 can1*Δ*::STE2pr-SpHIS5 lyp1*Δ *ura3Δ0 his3Δ1 LEU2 MET15*; strong constitutive expression of fluorescent proteins during exponential growth is achieved by carboxyl-terminal fusion to the Pdc1 protein.

For gene-drug interactions, a collection of mCherry-tagged gene-deletion strains was generated by mating an array of 85 strains from the yeast deletion collection to the *ho*Δ YEG01-RFP SGA-starter strain, as previously described [13]. Resulting prototrophic strains were *MAT*-a *x*Δ*::kanMX4 ho*Δ*::natMX4 PDC1-RFP.CaURA3MX4 can1*Δ*::STE2pr-SpHIS5 lyp1*Δ *ura3Δ0 his3Δ1 LEU2 MET15*. The CFP reference strain was the dual neutral marker reference *his3*Δ*::kanMX4 ho*Δ*::natMX4*. Double-marker

strains and CLS data were successfully obtained for 76 deletion strains (Supplementary Data S1).

Aging medium was synthetic complete (SC) with ammonium, 2% glucose, and 0.2% amino acid supplement mix (CSHL Manual, 2005), without buffering. 40mM metformin (Sigma D150959) was used where indicated. Single-culture and competitive outgrowth kinetics were done in low fluorescence YNB medium (YNB-lf) with 2% glucose and complete amino-acids supplement mix (Sigma Y1501 completed with Sigma U0750) [23]. All cultures were incubated in a growth chamber at 30 ºC and 80%-90% relative humidity without shaking; aging co-cultures were vigorously shaken at every sampling point. For media recipes, see Supplementary Table S1.

Competitive-aging culture setup and outgrowth measurements. To obtain relative CLS measurements, mutant ($x\Delta_{RFP}$) and reference strains (WT_{RFP} and WT_{CFP}) were pre-cultured separately until saturation. Saturated cultures were mixed in a 2:1 mutant:reference ratio and ~1.5 μL aliquots were transferred with a 96 solid-pin replicator (V&P Scientific VP 407) onto 96 semi deepwell plates (Nunc 260251) with 750 μL of fresh aging medium and disposable plastic covers.

Outgrowth sampling of the competitive-aging culture began 3 days after initial inoculation (time zero) and was repeated initially every 24 h and afterwards 48-72 h for up to 16 days after time zero. At each sampling day, T_i, 12 μL of shaken aging cultures were inoculated onto 140μL fresh YNB-lf medium in clear polystyrene 96-well plates (Corning 3585). Outgrowth was monitored every 1-3 h until cultures reached stationary phase, by measuring raw fluoresence of mCherry (*RFP*, Ex 587/5 nm and Em 610/5

nm), Cerulean (*CFP*, Ex 433/5 nm and Em 475/5 nm), and absorbance at 600 nm (OD_{600}) using a Tecan Infinite M1000 reader integrated to a robotic platform (Tecan Freedom EVO200). Outgrowth cultures were resuspended by vigorous shaking right before every measurement. To increase fluorescence-signal dynamic range, an outgrowth culture with the samples was measured one day before the actual experiment; optimal-gain was calculated at late exponential-growth, when fluorescence signal is at its maximum level. Optimal gain values were fixed for all measurements in the experiment; values used were 140-167 and 131-137 for *RFP* and *CFP*, respectively.

Death-rate calculation from competitive-aging outgrowth data. The $\frac{RFP}{CFP}$ signal ratio was used to estimate the number of cells expressing each fluorescent signal after subtracting auto fluorescence background defined as the *RFP* and *CFP* signal of WT_{CFP} and WT_{RFP} monocultures, respectively. Using data from different measurements in the outgrowth cultures (t_j, in hours) of each stationary-phase sampling point (T_i, in days), the signal ratio $ln\left(\frac{RFP}{CFP}\right)_{T_i,t_j}$ of each sample (w) was fitted to the linear model $A_w + S_w \cdot T_i + G_w \cdot t_j + C_{T_i,\,t_j}$, where A is the ratio of viable cells at the beginning of the experiment, S (relative survivorship) is the death-rate difference of the mutant and wild-type reference, and G (relative growth) is their growth-rate difference in the outgrowth co-culture. In addition, the term $C_{T_i,\,t_j}$ was introduced to consider the systematic variation of each plate at each stationary-phase sampling point $T_i t_j$. A complete description of the model and its implementation is provided in Supplementary Note S1.

Deriving gene-drug interactions from CLS phenotypes. To identify gene-drug interactions, namely cases in which the CLS phenotype of a gene-knockout strain is

significantly aggravated or alleviated by treatment with a drug, the relative survivorship of a set of 76 deletion strains was measured with and without 40 mM metformin. Deletion strains were randomly selected from the yeast deletion collection, considering only genes with a human orthologue (Ensembl). Relative survivorship values were rescaled to a dimensionless parameter, given that metformin increases yeast CLS [24,25] and that the relative survivorship S expressed in days is constrained by the death rate of the wild-type reference, r_{wt}, which will be different for each condition. For each mutant under a given condition, rescaled survivorship (rS) was defined as $rS = -\ln\left(1 - \frac{S}{r_{wt}}\right)$, where r_{wt} is the average death rate of all control wild-type competitions (WT_{RFP}+WT_{CFP}) in each plate. Gene-drug interactions were defined as cases in which a mutant's rS was significantly different between the SC and SC+metformin experiments (p<0.05; t-test).

Measuring death rate in monoculture from outgrowth kinetics. CLS estimates based on outgrowth kinetics of single-population aging cultures were adapted from a well established high-throughput method [21,22]. Culture density was monitored by increase in absorbance at OD_{600nm} after subtracting background signal, defined as OD_{600} at outgrowth inoculation, to each data point. At each aging sampling point T_i (days), the time-delay in hours, t, to reach a fixed cell density of OD_{600}=0.35 reports for the remaining fraction of viable cells in the population, as previously reported [21]. Specifically, for each successive age time point, the percent of viability (V_T) was calculated using the equation $V_T = \frac{1}{2(\Delta \mathrm{t}_n/\delta)}$, where $\Delta \mathrm{t}_n$ is the time shift and δ is the doubling time. Death rates were obtained from the exponential decay rate calculated by

fitting all V_T data points as a function of time in stationary phase to a first-order exponential model (Matlab, fit).

Flow cytometry analysis. Outgrowth cultures were sampled once at eight hours after inoculation. A flow cytometer with a high-throughput sampler (LSRFortessa-HTS, Becton Dickinson) was used to record fluorescence from CFP and RFP fluorophores. CFP was excited with a 405nm violet laser, and fluorescence signal was collected through a 450/50 nm band-pass filter. RFP was excited with a 561nm yellow-green laser, and fluorescence was collected through a 610/20 nm band-pass filter and a 600LP emission filter; 10µL of culture were measured at a flow rate of 1 µl/s. For each well, data analysis was carried out as follows: First, the smallest number of events of the four age sampling points was taken and the same number of randomly selected events were used for the other three sampled time points, T. Next, fluorescent signals (xFP) were normalized as $NormFluor = xFP - \min(xFP)/\max(xFP) - \min(xFP)$, where $\min(xFP)$ is the value of the event in the 0.1 bottom percentile of the log10(x*FP*) signal.

RESULTS

Relative survivorship in stationary phase can be estimated from bulk fluorescence signal of two populations in co-culture

We sought to test and to improve a competition-based method to describe CLS phenotypes in budding yeast. To directly measure the lifespan effects of gene deletions, we tracked changes in the relative abundances of viable RFP- and CFP-tagged deletion ($x\Delta_{RFP}$) and wild-type strains (WT_{CFP}), respectively, as a function of time in stationary

phase (*T*, days) in co-culture (**Figure 1A**). To this end, we inoculated stationary-phase cells at different time points into fresh medium and monitored the outgrowth at multiple times (*t*, hours) by measuring absorbance at 600nm (OD_{600}), bulk RFP signal (*RFP*), and bulk CFP signal (*CFP*), until the outgrowth co-cultures reached saturation. First, we characterized the CLS of nine deletion strains that are known to show increased or decreased lifespan [5,12,13,15,26–28]. Each RFP-tagged deletion strain was co-cultured with the WT_{CFP} reference in up to seven replicates in a single deep-well plate, until saturation (see Materials and Methods). Competitive-aging cultures were monitored for ~15 days in stationary phase.

As expected, outgrowth kinetics measured by OD_{600} showed a clear shift with time (days) in stationary phase; aging co-cultures gradually took a longer time in outgrowth (hours) to reach a given cell density (**Figure 1B**). This overall shift in growth kinetics reflects the loss of viability with age, as previously described [21]. In terms of fluorescence-signal kinetics, we observed that the WT_{RFP} or WT_{CFP} monocultures mostly recapitulated OD_{600} kinetics, suggesting that loss of viability can also be measured by the shift in time of the fluorescence signal (**Figure 1B**, red and blue lines). WT_{RFP}+WT_{CFP} populations competed in co-culture showed similar shifts in fluorescence signals, suggesting that loss of viability occurred at similar rates in both WT populations, as expected (**Figure 1B**, gray lines). In contrast, some $x\Delta_{RFP}$+WT_{CFP} co-cultures showed delayed or exacerbated shifts in fluorescence kinetics. For instance, the *hap3*Δ_{RFP}+WT_{CFP} co-culture showed a steep decrease in bulk RFP signal along with a slight increase in bulk CFP signal, as a function of days in stationary phase (**Figure 1B**,

green lines). This suggests that loss of viability in the *hap3*Δ_{RFP} population occurred at a faster rate than in the WT_{CFP} reference, indicating a short-lifespan phenotype for *hap3*Δ.

In our bulk-fluorescence measurement setup, the observed changes in fluorescence kinetics could reflect a drop of either the number of cells expressing a fluorescent protein or the florescent-protein expression level in the outgrowth cultures with time in stationary phase. To discriminate between these two scenarios, we used flow cytometry to directly measure the fraction of cells expressing RFP or CFP. We observed that the previously observed changes in bulk fluorescence signal in co-culture were in agreement with changes in the number of tagged cells (**Figure 1C**; see Supplementary Figure S1 for all strains tested). The typical fluorescence per cell remained constant throughout the experiment for both *RFP* and *CFP* signals, for all deletion strains tested. These results indicate that changes in bulk-fluorescence kinetics in outgrowth cultures is a good estimator of the number of fluorescent cells; therefore, bulk fluorescence in co-culture can be used to estimate loss of cell population viability as a function of time in stationary phase.

A model to adjust relative survivorship in co-culture from changes in relative fluorescence signal

To obtain a quantitative phenotypic value from our experimental measurements, we developed a model that provides a relative survivorship parameter (S). Specifically, we established a multiple linear regression analysis where each experimental measurement in the outgrowth culture is modeled as:

$$ln\,(\frac{RFP}{CFP})_{T_i,\,t_j} = A_w + S_w \cdot T_i + G_w \cdot t_j + C_{T_i,\,t_j}$$

Using a system of linear equations, we obtained the regression coefficients using all outgrowth measurements in a 96-well plate. The contribution of relative survivorship (S) along with the other three parameters for competing populations are illustrated in **Figure 1D** and Supplementary Figure S2. The expected value, $ln\,(\frac{RFP}{CFP})_{T_i,\,t_j}$, is the logarithmic quotient of the sizes of the populations of $x\Delta_{RFP}$ and WT_{CFP} from an outgrowth inoculated at day T_i in stationary phase and measured after t_j hours in the outgrowth culture (Supplementary Note S1). The parameter A_w is the logarithmic proportion of the sizes of both populations at the beginning of the experiment (**Figure 1D** , solid vertical lines at $T_1 = 0$). The difference in death rates is S (**Figure 1D**, linear regression, open circles), while G is the difference in growth rates (linear regression, crosses). The term $C_{T_i,\,t_j}$ is the error in each measurement, which is mostly determined by the deviation from zero change in WT_{RFP}+WT_{CFP} reference competitions, and is similar to the deviation of measurements in $x\Delta_{RFP}$+WT_{CFP} competitions (Supplementary Figure S2). The rationale here is that relative survivorship (S) and relative growth rate (S) are by definition equal to zero in reference competitions (WT_{RFP}+WT_{CFP}), and therefore consistent changes in $ln\,(\frac{RFP}{CFP})$ are likely due to systematic errors in the measurements. It must be noted that there are usually survivorship and growth-rate differences between the two wild-type strains (WT_{RFP} and WT_{CFP}), which are also taken into account while fitting the data.

This data analysis procedure is a more exhaustive description of the actual competitive-aging setup, compared to our original report (Garay et al. 2014). Specifically, it takes

into account relevant parameters fitting the measured data and has fewer assumptions, in particular we explicitly described the difference in growth rates between both strains in the outgrowth cultures using the parameter G, so the quantification of relative survivorship is not biased by growth-rate phenotypes. We also consider systematic measurement errors by including the C_{T_i, t_j} term. In the following sections, we show that competitive-aging experiments with multiple-regression modeling provide reliable quantifications of relative survivorship, which are useful to identify CLS phenotypes and to score their interactions with environmental factors.

Competitive-aging experiments provide replicable estimates of survivorship despite inter-batch variation

To systematically assess the technical replicability of the competitive-aging method, we measured the CLS of nine mutants and reference strains in 96-well plates with multiple independent replicate wells. Specifically, we measured CLS of up to seven replicate samples of each one of the nine deletion mutants together with 31 wild-type reference competitions in a 96-well plate (**Figure 2A**); the entire experiment was carried out twice (two experimental batches). We validated our results with another large-scale method that provides precise estimates of survivorship (**Figure 2B**). In particular, we measured CLS of the same array of mutants and wild-type strains using an established high-throughput method that is based in the changes of outgrowth kinetics of aging monocultures [21,22]. Qualitative inspection showed that both methods scored mutants with known CLS effects [26,29], such as *rim15*Δ and *hap3*Δ that resulted in reduced survivorship, and *ras2*Δ showing increased lifespan compared to wild type.

To quantitatively contrast the replicability of both experimental approaches, we fitted decay curves from the outgrowth kinetics experiments to an exponential model. We then compared the difference of adjusted exponential death rates of wild-type and mutant strains from monoculture aging to the S parameter obtained from competitive-aging. We observed that both methods performed similarly when comparing the technical variation within each of the experimental batches; there was no significant difference in the typical standard error of the mean in outgrowth kinetics and competitive aging (Supplementary Figure S3). However, when looking at the correlation of quantitative data resulting from independent experiments, we found that the correlation was remarkably higher when experiments were done with the competitive-aging approach (**Figure 2C**; r^2=0.56 and r^2=0.94 for outgrowth kinetics and competitive aging, respectively, Pearson correlation). We note that one of the outgrowth-kinetics experiments was atypically noisy for *ras2*Δ (not shown); hence this strain was excluded in the analysis, as it would overestimate the intra- and inter-batch variability of the outgrowth-kinetics approach. Together, these results indicate that the competition-based method is highly replicable, despite the inherent variation of different experimental batches.

We looked closer into the the diminished replicability of the outgrowth-kinetics method and compared the distribution of effects of all deletion mutants in both batches, as determined by the two experimental approaches (**Figure 2D**). Deletions *rim15*Δ and *hap3*Δ showed short-lived phenotypes with high statistical support in all experiments. Conversely, the short-lived phenotypes of *ste12*Δ, *msn4*Δ, *msn2*Δ, and *atg1*Δ were consistently detected only by competitive-aging but not by monocultures, in which short-

lived phenotypes were only scored in one of two experimental batches. Long-lived phenotypes were identified in both approaches, but competitive-aging screening had better resolution, with better statistical support for the long-lifespan phenotype of the *swr1*Δ strain (*p*-val<10^{-9} in both batches, *t*-test).

Having multiple reference samples (WT_{RFP}+WT_{CFP}) in the 96-well plate improves the fit of the model, but reduces the throughput for large-scale studies, which usually require many independent experimental batches. To maximize throughput without losing quantitative resolution, we used this experiment to estimate the number of reference samples per plate that are required for a reliable estimate of S. To do so, we quantified how the variation of mutant samples depended on the number of WT references (31 in this experiment) used to fit S=0. We observed that both the standard deviation of S of the average sample and the confidence intervals of the fit of S showed a steep decline from one to five reference samples, after which variation kept decreasing, with diminishing returns (Supplementary Figure S4). Thus, including 6-10 reference samples are enough to provide a robust description of relative-CLS phenotypes in large-scale genetic analyses of mutants, environments, and their interactions.

Competitive-quantification of CLS under different conditions successfully describes gene-drug interactions

Lifespan is a complex trait determined by different cellular pathways, hundreds of genes, and environmental variables [2,31]. A current challenge in the field is to understand how different factors are integrated with one another to control cell survivorship. Our competitive-aging method provides high-resolution and replicable data, which enables a

quantitative description of CLS-phenotype interactions. As a proof of principle, we screened for gene-environment interactions in an array of knockout mutants aged with and without the lifespan-extending drug metformin.

We confirmed that the CLS of WT reference samples of yeast increased significantly from a half life of 10.7 to 15.5 days when treated with 40mM metformin (**Figure 3A**; $p<10^{-9}$, Wilcoxon rank sum test). Next, we used our competitive-aging approach to measure the CLS of an array of 76 knockout strains aged with or without metformin. In both conditions, we observed high quantitative correlation of the phenotypes between replicate plates in the same experiment and between two independent experiments (Supplementary Figure S5). A direct quantitative comparison of CLS phenotypes under both conditions is shown in **Figure 3B** (see Supplementary Figure S6 for data rescaling). Most samples were found to fall close to the diagonal; namely the phenotypic effect of the knockout relative to WT was similar under both conditions. However, the phenotypes of 17 of the 76 knockouts (22%) were significantly different when treated with metformin (*t*-test, $p<0.05$; **Figure 3C**); these are potential gene-drug interactions.

For the most extreme differential phenotypes, we show the modeled change in relative survivorship as a function of age (**Figure 3D**). In many cases, we observed that metformin alleviated or even reverted the short-lifespan effects of the gene deletion, with *pep1*Δ, *die2*Δ, and *alg3*Δ being the most extreme instances. In only one mutant, *lsc2*Δ, the drug significantly aggravated the short-lived gene-deletion phenotype. On the opposite scenario, the nominal long-lived phenotype of certain mutants was rendered neutral or closer to neutral with the metformin treatment (eg. *hsv2*Δ, *ubp13*Δ, and

*ubp5*Δ). The identified gene-drug interactions, with specific quantitative information on the magnitude and sign of the effects, constitute a powerful means to pinpoint the underlying mechanisms of longevity by metformin in yeast.

Finally, we used the data set of 76 knockout strains to evaluate the influence of mutant's growth rate in the context of our competitive-aging method and multiple-regression model, which includes parameter G. Importantly, we observed that the model correctly identified mutants with growth defects, as reported in the literature (Supplementary Figure S7); hence, this parameter may enhance a more accurate quantification of relative survivorship of deletion strains. The data was fitted to G assuming G=0; we observed that the difference in the estimation of S when G was included was modest, but mostly explainable by G. As expected, the relative survivorship of slow-growth mutants was usually underestimated when differences in growth rate were not taken into account (Supplementary Figure S7). Together, results in this section show that competitive-aging yields accurate and replicable large-scale CLS data, providing valuable information to shed light on the mechanisms of pharmacological interventions that extend lifespan.

DISCUSSION

Genetic analysis of the CLS of budding yeast has led to the genome-wide identification of genes involved in aging; recent efforts have sought to describe interactions between genetic and environmental modulators of the phenotype [13,15–17]. A previous report from our group has shown some advantages of using a competitive-aging approach, in which

fluorescently-labeled strains in co-culture provide high resolution in parallel setups [13]. Competitive-aging has also allowed scoring gene-environment interactions at the genomewide level, specifically interactions with dietary restriction [15]. Here, we have introduced a new model to calculate the relative survivorship of deletion strains, taking into account the possible confounding effects coming from growth-rate differences and systematic batch effects. In addition, we directly quantitatively compared the performance of a competitive-aging setup to an established approach [21,22]. CLS phenotypes were successfully recapitulated with both approaches, but competitive-aging provided higher replicability and resolution. With this enhanced method and data analysis, we were able to unravel significant gene-drug interactions in an array of 76 deletions strains subjected to the lifespan-extending drug metformin.

Early CLS genome-wide screens were based on large pools of gene deletions followed by molecular-barcode hybridization or sequencing [10,11,14]. These studies provided important insight into which genetic factors mediate stationary phase survival, such as autophagy, vacuolar protein sorting, and regulation of translation. However, the high rates of false positives—specially in the cases of long-lived phenotypes—and low overlap among the sets of genes from different studies [17] suggest that systematic errors in barcode detection or major experimental batch effects result in poor experimental replicability. On the other side of the spectrum, an ingenious outgrowth-kinetics approach of yeast monocultures increases the feasibility of percent-survivorship estimates, compared to the conventional colony-forming units method [21]; but throughput is still limited with this approach. To overcome this limitation, Jung and co-workers scaled-up this strategy using monocultures in multi-well plates, whereby more strains

can be tested in parallel [16,22]. There is still the issue that mild environmental variation can affect separate cultures differently, that could lead to low reproducibility [12]; for instance, strains may reach stationary phase at different times after inoculation. In this regards, competitive-aging provides a direct phenotypic comparison and, arguably, more consistent results, given that the mutant population of interest is aged with an internal reference strain under the exact same microenvironment. Importantly, competitive-aging can also be carried out in multi-well plates, enabling high-throughput experimental setups.

Results herein presented confirmed that, in our hands, CLS phenotypes replicated better when obtained by competitive-aging and multiple-regression modeling using several predictor variables such as relative survivorship, relative growth-rate, initial frequency, and systematic biases in batch measurements. While the degree of agreement between measurements conducted on replicate samples in different laboratories remains to be addressed, it is likely that competitive-aging could provide higher reproducibility for the field of yeast CLS genetics. One of the inherent drawbacks of the method is that no absolute death-rate information is provided, which can be easily solved thorough characterization of the wild-type strain in monoculture, as we have shown. Likewise, the dynamic range of this method depends on the actual death rate of the reference strain used. For instance, quantitative phenotypic descriptions are limited if S>>0; in other words only semi-quantitative estimates are possible for extremely long-lived strains ($S \approx r_{wt}$). The use of different reference strains, eg. specific gene deletions with known long-lifespan phenotypes, may help to overcome this limitation. In addition, just as most population-based CLS methods, competitive aging depends on cells being

able to re-enter the cell cycle, which can only be distinguished from actual death using outgrowth-independent methods, such as live/dead staining.

We have illustrated the potential of competitive-aging screening by characterizing an array of yeast deletion strains exposed to metformin. A number of lifespan-extending pharmacological interventions are already being tested for age-related diseases in humans, even when the mechanisms underlying their beneficial effects are frequently not fully understood [32,33]. Given that lifespan is a complex phenotype, identifying conserved gene-drug interactions could shed light on the modes of action and to pinpoint genetic modifiers of the drug's effects [33]. By screening an array of 76 gene deletions aged with metformin, we found a number of cases in which metformin buffers both short- or long-lifespan mutant phenotypes. The interacting genes suggest a role of protein glycosilation and protein homeostasis, which is in line with previous evidence showing that metformin alters glycation, protein transport, and protein degradation in yeast [24,34]. Our results also uncovered interactions between metformin and genes involved in mitochondrial function (*erp6*Δ, *lsc2*Δ*, ema35*Δ, *sap155*Δ, and *ylh47*Δ), which is a known player in the cellular response to metformin [24,25]. It remains to be addressed how these proteins are specifically related to the known response involving the mitochondrial electron transport chain and homeostasis of copper and iron.

Competitive-aging can readily be adapted to screen double mutants at large scale and to score genetic interactions underlying CLS phenotypes. A proof-of-principle study suggests that positive (alleviating) genetic interactions are common between short-lifespan autophagy mutants [13]. Genetic interactions (epistasis) are a powerful tool to describe the architecture of phenotypes and the functional relationships of different

genetic pathways [35–39]. While epistasis-network analyses in yeast have granted deep knowledge of the genetic landscape of mitotically-active, proliferating cells, less is known about how genetic interactions shape the genetic architecture of post-mitotic survivorship. Large-scale genetic analysis of double-mutants aged in competition with their single-mutant references is an attractive experimental setup to identify interactions among different genes and pathways underlying CLS in yeast. Our competitive-aging screening method and quantitative analysis provide a powerful systematic tool to shed light on the complex genetic, environmental, and pharmacological wiring of aging cells.

Acknowledgements

We are grateful to Erika Cruz-Bonilla, Nelly Selem, and Judith Ulloa for critical reading of the manuscript. This work was funded by grants to A.D. from the Consejo Nacional de Ciencia y Tecnología de México (CONACYT grants CB-2015/164889 and PN-2016/2370) and the Consejo de Investigación sobre Salud y Cerveza de México. J.A.A.-R. received a doctoral fellowship from CONACYT (#264529). The funders had no role in study design, data collection and analysis, decision to publish, or preparation of the manuscript.

Author Contributions

Conceived and designed the study: JAA-R, AD. Performed the experiments: JAA-R, MM-F, AJ-R, EG, SEC. Developed and implemented the model: JAA-R, EG, NS. Analyzed the data: JAA-R, SEC, AD. Wrote the paper: JAA-R, AD. Acquired funding:

AD. All authors read and approved the final version All authors read and approved the final version of the submitted manuscript.

Conflict of interest

The authors declare that they have no competing interests.

LIST OF SUPPLEMENTARY ITEMS

Note S1. Supplementary Note 1. Development and implementation of a linear model to calculate relative survival of mutant strains in competitive-aging cultures.

Table S1. Recipes for media used in this study.

Figure S1. The change in the RFP and CFP events detected by flow cytometry in outgrowth cultures reflects differential death rates.

Figure S2. Contribution of the parameter *C* (systematic measurement error) to fitted time points.

Figure S3. Equivalent intra-batch variation of survivorship measured by the competitive-aging and OD-based outgrowth-kinetics approaches.

Figure S4. Increasing the number of reference samples within an experimental batch reduces variation in relative survivorship (*S*).

Figure S5. Relative survivorship (*S*) is well replicated between plates within the same experimental batch, as well as between different batches.

Figure S6. Relative survivorship (*S*) was transformed to the dimensionless, rescaled parameter *rS*.

Figure S7. The *G* parameter corrects effects of differential growth rates that otherwise underestimate relative survivorship.

Data S1. Array of mutants used for gene-drug interactions, with their relative survivorship, rescaled survivorship, and relative growth rates.

REFERENCES

1. Kirkwood TBL. A systematic look at an old problem. *Nature.* 2008;451(7179):644-647.
2. López-Otín C, Blasco MA, Partridge L, Serrano M, Kroemer G. The Hallmarks of Aging. *Cell*. 2013;153(6):1194-1217.
3. Longo VD, Fabrizio P. Chronological aging in Saccharomyces cerevisiae. *Subcell Biochem*. 2012;57:101-121.
4. Eisenberg T, Knauer H, Schauer A, et al. Induction of autophagy by spermidine promotes longevity. *Nat Cell Biol*. 2009;11(11):1305-1314.
5. Wei M, Fabrizio P, Hu J, et al. Life span extension by calorie restriction depends on Rim15 and transcription factors downstream of Ras/PKA, Tor, and Sch9. *PLoS Genet*. 2008;4(1):0139-0149.
6. Gems D, Partridge L. Genetics of Longevity in Model Organisms: Debates and Paradigm Shifts. *Annu Rev Physiol*. 2013;75(1):621-644.
7. Longo VD, Shadel GS, Kaeberlein M, Kennedy B. Replicative and Chronological Aging in Saccharomyces cerevisiae. *Cell Metab*. 2012;16(1):18-31.
8. Hu J, Wei M, Mirisola MG, Longo VD. Assessing Chronological Aging in Saccharomyces cerevisiae. In: Humana Press, Totowa, NJ; 2013:463-472.
9. Powers RW, Kaeberlein M, Caldwell SD, Kennedy BK, Fields S, Fields S. Extension of chronological life span in yeast by decreased TOR pathway signaling. *Genes Dev*. 2006;20(2):174-184.
10. Matecic M, Smith DL, Pan X, et al. A Microarray-Based Genetic Screen for Yeast Chronological Aging Factors. Kim SK, ed. *PLoS Genet*. 2010;6(4):e1000921.
11. Fabrizio P, Hoon S, Shamalnasab M, et al. Genome-Wide Screen in Saccharomyces cerevisiae Identifies Vacuolar Protein Sorting, Autophagy, Biosynthetic, and tRNA Methylation Genes Involved in Life Span Regulation. *PLoS Genet*. 2010;6(7):e1001024.
12. Burtner CR, Murakami CJ, Olsen B, Kennedy BK, Kaeberlein M. A genomic analysis of chronological longevity factors in budding yeast. *Cell Cycle*. 2011;10(9):1385-1396.
13. Garay E, Campos SE, González de la Cruz J, Gaspar AP, Jinich A, DeLuna A. High-Resolution Profiling of Stationary-Phase Survival Reveals Yeast Longevity Factors and Their Genetic Interactions. *PLoS Genet*. 2014;10(2):e1004168.
14. Gresham D, Boer VM, Caudy A, et al. System-level analysis of genes and functions affecting survival during nutrient starvation in Saccharomyces cerevisiae. *Genetics*. 2011;187(1):299-317.
15. Campos SE, Avelar-Rivas JA, Garay E, Juárez-Reyes A, DeLuna A. Genomewide mechanisms of chronological longevity by dietary restriction in budding yeast. *Aging Cell*. 2018;17(3):e12749.
16. Jung PP, Zhang Z, Paczia N, et al. Natural variation of chronological aging in the Saccharomyces cerevisiae species reveals diet-dependent mechanisms of life span control. *npj Aging Mech Dis*. 2018;4(1):3.

17. Smith DL, Maharrey CH, Carey CR, et al. Gene-nutrient interaction markedly influences yeast chronological lifespan. *Exp Gerontol*. 2016;86:113-123.
18. Burtner CR, Murakami CJ, Kennedy BK, Kaeberlein M. A molecular mechanism of chronological aging in yeast. *Cell Cycle*. 2009;8(8):1256-1270.
19. Santos J, Leitão-Correia F, Sousa MJ, Leão C. Ammonium is a key determinant on the dietary restriction of yeast chronological aging in culture medium. *Oncotarget*. 2015;6(9):6511-6523.
20. Campos SE, DeLuna A. Functional genomics of dietary restriction and longevity in yeast. *Mech Ageing Dev*. 2019;179:36-43.
21. Murakami CJ, Burtner CR, Kennedy BK, Kaeberlein M. A Method for High-Throughput Quantitative Analysis of Yeast Chronological Life Span. *Journals Gerontol Ser A Biol Sci Med Sci*. 2008;63(2):113-121.
22. Jung PP, Christian N, Kay DP, Skupin A, Linster CL. Protocols and Programs for High-Throughput Growth and Aging Phenotyping in Yeast. *PLoS One*. 2015;10(3):e0119807.
23. Sheff MA, Thorn KS. Optimized cassettes for fluorescent protein tagging inSaccharomyces cerevisiae. *Yeast*. 2004;21(8):661-670.
24. Borklu-Yucel E, Eraslan S, Ulgen KO. Transcriptional remodeling in response to transfer upon carbon-limited or metformin-supplemented media in S. cerevisiae and its effect on chronological life span. *Appl Microbiol Biotechnol*. 2015;99(16):6775-6789.
25. Stynen B, Abd-Rabbo D, Kowarzyk J, et al. Changes of Cell Biochemical States Are Revealed in Protein Homomeric Complex Dynamics. *Cell*. 2018;175(5):1418-1429.e9.
26. Fabrizio P, Longo VD. The chronological life span of *Saccharomyces cerevisiae*. *Aging Cell*. 2003;2(2):73-81.
27. Alvers AL, Fishwick LK, Wood MS, et al. Autophagy and amino acid homeostasis are required for chronological longevity in *Saccharomyces cerevisiae*. *Aging Cell*. 2009;8(4):353-369. doi:10.1111/j.1474-9726.2009.00469.x
28. Laschober GT, Ruli D, Hofer E, et al. Identification of evolutionarily conserved genetic regulators of cellular aging. *Aging Cell*. 2010;9(6):1084-1097.
29. Fabrizio P, Pozza F, Pletcher SD, Gendron CM, Longo VD. Regulation of Longevity and Stress Resistance by Sch9 in Yeast. 2001.
30. Kenyon CJ. The genetics of ageing. *Nature*. 2010;464(7288):504-512.
31. Yanai H, Budovsky A, Barzilay T, Tacutu R, Fraifeld VE. Wide-scale comparative analysis of longevity genes and interventions. *Aging Cell*. 2017;16(6):1267-1275.
32. Mullard A. Anti-ageing pipeline starts to mature. *Nat Rev Drug Discov*. 2018;17(9):609-612.
33. Zimmermann A, Hofer S, Pendl T, Kainz K, Madeo F, Carmona-Gutierrez D. Yeast as a tool to identify anti-aging compounds. *FEMS Yeast Res*. 2018;18(6).
34. Kazi RS, Banarjee RM, Deshmukh AB, Patil G V., Jagadeeshaprasad MG, Kulkarni MJ. Glycation inhibitors extend yeast chronological lifespan by reducing advanced glycation end products and by back regulation of proteins involved in

mitochondrial respiration. *J Proteomics*. 2017;156:104-112.

35. Segrè D, DeLuna A, Church GM, Kishony R. Modular epistasis in yeast metabolism. *Nat Genet*. 2005;37(1):77-83.
36. Onge RPS, Mani R, Oh J, et al. Systematic pathway analysis using high-resolution fitness profiling of combinatorial gene deletions. *Nat Genet*. 2007;39(2):199-206.
37. Collins SR, Miller KM, Maas NL, et al. Functional dissection of protein complexes involved in yeast chromosome biology using a genetic interaction map. *Nature*. 2007;446(7137):806-810.
38. Phillips PC. Epistasis — the essential role of gene interactions in the structure and evolution of genetic systems. *Nat Rev Genet*. 2008;9(11):855-867.
39. Kuzmin E, VanderSluis B, Wang W, et al. Systematic analysis of complex genetic interactions. *Science.* 2018;360(6386).

FIGURE LEGENDS

Figure 1. Measuring relative survivorship using a competitive-aging approach. *A*, Schematic of the experimental setup. A co-culture of fluorescence-tagged gene deletion ($x\Delta_{RFP}$) and wild-type reference (WT_{CFP}) strains in stationary phase is sampled regularly at days T. Outgrowth cultures in fresh medium are monitored at t hours with simultaneous measurement of absorbance at 600nm (OD_{600}), and raw *RFP* and *CFP* signals. Change in fluorescent-signal ratio in the outgrowth cultures is used to estimate the relative number of viable cells after T days in stationary phase. Possible differences in growth rate (*G*) are taken into account. ***B,*** Raw data of OD_{600}, *RFPraw* and *CFPraw* signal from outgrowth cultures; specific examples with only WT_{RFP} (red lines), only WT_{CFP} (blue lines), and both WT cells in co-culture (WT_{RFP}+WT_{CFP}, gray lines) are shown. Last column shows one deletion strain in co-culture with the wild type, WT_{CFP}+*hap3*Δ_{RFP} (green lines). Although samples are measured throughout the outgrowth culture after inoculation, analysis only considers data points at exponential growth (grayscale circles). ***C,*** Frequency of *RFP* and *CFP* signals in all events measured by flow cytometry from outgrowth cultures at four age time points T, including the first and last days of the experiment. ***D,*** Description of how the different parameters fit data to the linear model. Points are the experimental determinations of ln(*RFP/CFP*). For each well, parameter A indicates the deviation from ln(*RFP/CFP*)=0 at T=0. Crosses shown directly above experimental data are the fitted data $ln\,(\frac{RFP}{CFP})_{T_i,\,t_j}$ at the time of each measurement; their linear regression has slope G (the relative growth rate). Open circles are the data fitted at T_i; error bars at those time points are the 95% CI of the fit; their linear regression has slope S (the relative survivorship, our parameter of interest). Parameter C of the model (not plotted) is the fitted batch error of each measurement (see Supplementary Figure S2).

Figure 2. The competitive-aging method is accurate and replicable. *A*, Relative survivorship estimated by competitive aging. The modeled ln(*RFP*/*CFP*) is shown for the WT and nine mutant strains at each T_i point, averaged for 6-7 technical replicates. Error bars are the S.E.M. ***B***, Percent of surviving cells in monoculture over time

measured by the shift in outgrowth kinetics. Mean and the S.E.M. from 6-7 technical replicates are shown. ***C***, Relative survivorship is shown for two experimental batches, expressed either as the difference of individual death rates ($r_{wt} - r_x$, black) for monoculture outgrowth kinetics or as survivorship coefficients (S, red) for competitive aging. Each data point is one of the 6-7 technical replicates of monocultures or competitions (31 for replicates of the WT strain). Horizontal lines are the mean of each data series. The *ras2*Δ strain was only measured by outgrowth kinetics in one experimental batch. WT reference samples are not shown for the competitive-aging setup (by definition, S=0). Statistical differences between the distribution of S of each mutant and the WT reference within the same replicate and batch are shown (**p*<0.05, ***p*<0.01, ****p*<0.005, *n.s.* not significant; *t*-test). To obtain a distribution of WT references for statistic analysis of competitive aging, the S of each WT reference was calculated as an additional sample when fitting the model. ***D***, Correlation of replicate batch measurements of the competitive-aging (left) and monoculture outgrowth-kinetics (right) setups.

Figure 3. Identification of gene-drug interactions by competitive-aging screening. ***A***, Plot shows the half life of WT reference samples with or without metformin (*n*=40, ten per experiment). ***B***, Scatter plot comparing CLS phenotypes of 76 gene-deletion strains with or without metformin; shown is the average rescaled relative survivorship rS of four replicates (see Supplementary Figure S6). ***C***, Plot shows individual and average measurements of rS of strains with differential phenotypic effects (*p*<0.05, *t*-test). Gray diagonal lines are used to visualize the sign of the gene-drug interaction. ***D***, Modeled change in the relative proportion of surviving fluorescently-tagged knockout and WT strains. Solid lines show the mean of four replicates (dotted lines); the gray area is the 95% CI.

Figure 1

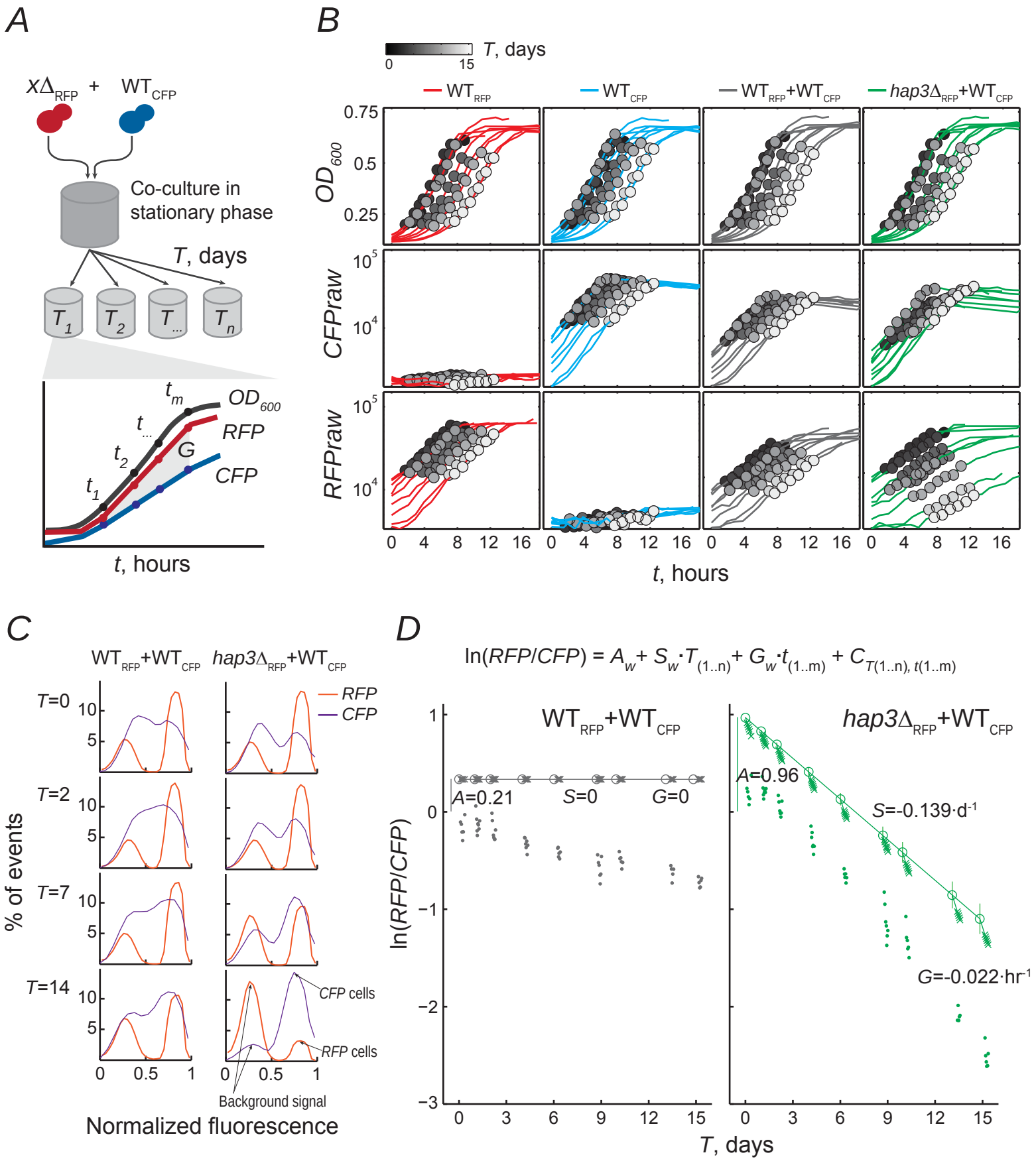
A
xΔRFP + WTCFP
Co-culture in stationary phase
T, days
T1
T2
T...
Tn
tm
OD600
t...
RFP
t2
G
CFP
t1
t, hours
B
T, days
0
15
WTRFP
WTCFP
WTRFP+WTCFP
hap3ΔRFP+WTCFP
OD600
0.75
0.5
0.25
CFPraw
RFPraw
10^5
10^4
0 4 8 12 16
t, hours
C
WTRFP+WTCFP
hap3ΔRFP+WTCFP
RFP
CFP
T=0
T=2
T=7
T=14
% of events
CFP cells
RFP cells
Background signal
Normalized fluorescence
D
ln(RFP/CFP) = Aw + Sw·T(1..n) + Gw·t(1..m) + CT(1..n), t(1..m)
WTRFP+WTCFP
hap3ΔRFP+WTCFP
A=0.21
S=0
G=0
A=0.96
S=-0.139·d-1
G=-0.022·hr-1
ln(RFP/CFP)
T, days

Figure 2

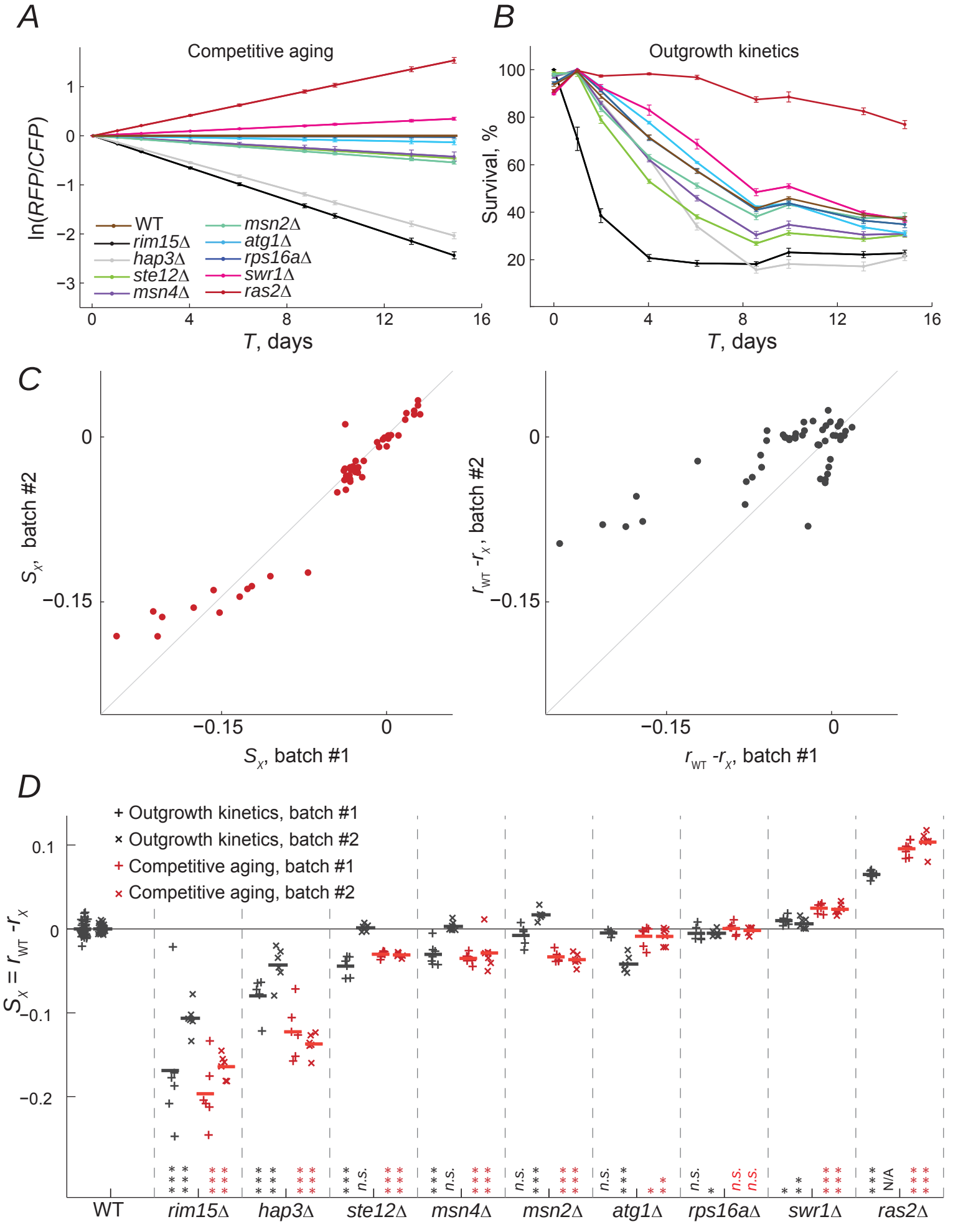
A
Competitive aging
ln(RFP/CFP)
T, days
WT
rim15Δ
hap3Δ
ste12Δ
msn4Δ
msn2Δ
atg1Δ
rps16aΔ
swr1Δ
ras2Δ
B
Outgrowth kinetics
Survival, %
T, days
C
S_X, batch #2
S_X, batch #1
r_WT -r_X, batch #2
r_WT -r_X, batch #1
D
+ Outgrowth kinetics, batch #1
× Outgrowth kinetics, batch #2
+ Competitive aging, batch #1
× Competitive aging, batch #2
S_X = r_WT -r_X
n.s.
N/A
WT
rim15Δ
hap3Δ
ste12Δ
msn4Δ
msn2Δ
atg1Δ
rps16aΔ
swr1Δ
ras2Δ

Figure 3

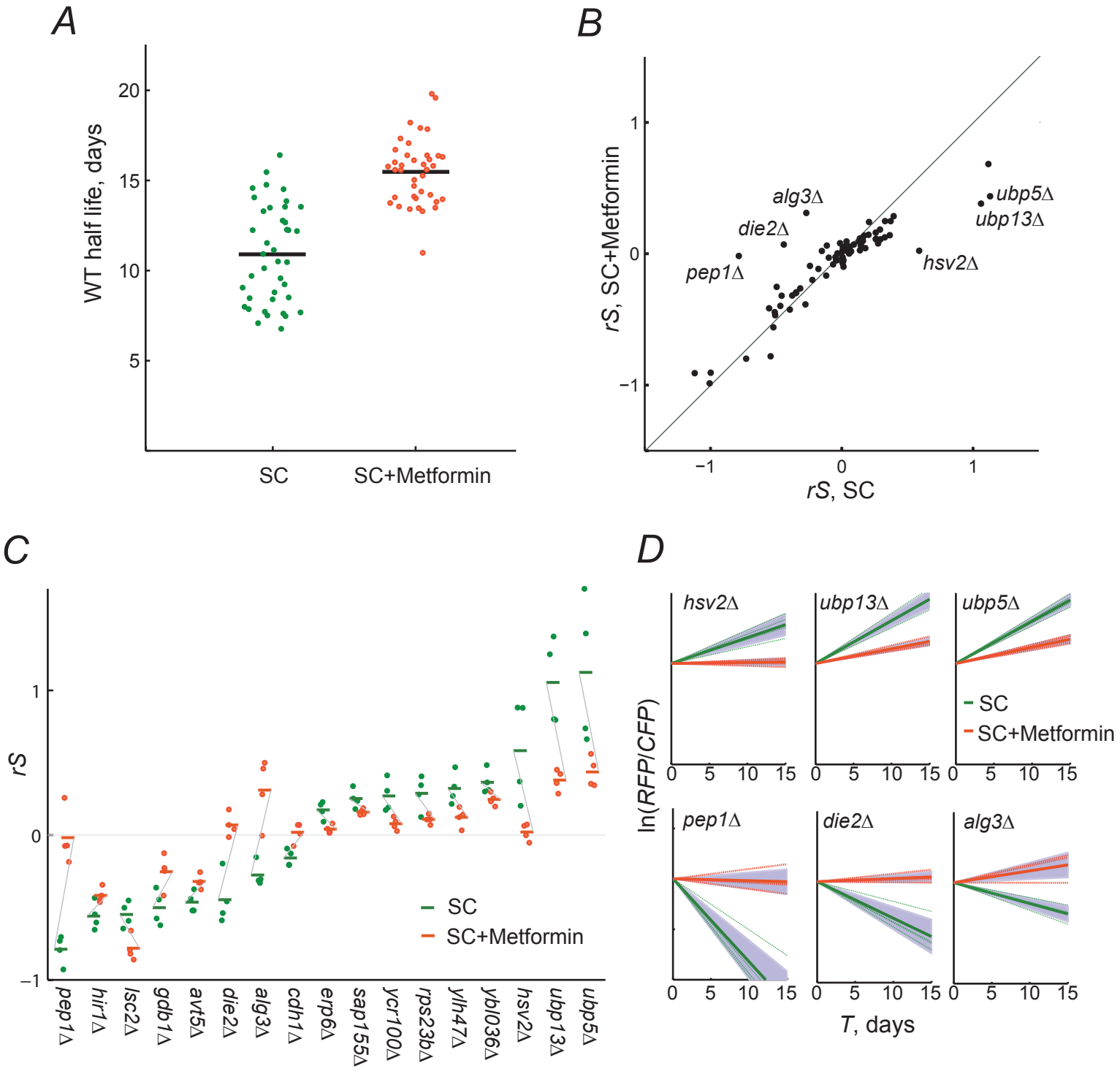
A
WT half life, days
20
15
10
5
SC
SC+Metformin
B
rS, SC+Metformin
rS, SC
1
0
−1
alg3Δ
die2Δ
pep1Δ
ubp5Δ
ubp13Δ
hsv2Δ
C
rS
1
0
−1
SC
SC+Metformin
pep1Δ
hir1Δ
lsc2Δ
gdb1Δ
avt5Δ
die2Δ
alg3Δ
cdh1Δ
erp6Δ
sap155Δ
ycr100Δ
rps23bΔ
ylh47Δ
ybl036Δ
hsv2Δ
ubp13Δ
ubp5Δ
D
ln(RFP/CFP)
hsv2Δ
ubp13Δ
ubp5Δ
SC
SC+Metformin
pep1Δ
die2Δ
alg3Δ
0
5
10
15
T, days